Inorganic Chemistry

ARTICLE

pubs.acs.org/IC

Hydrothermal Tm^{3+}—Lu_2O_3 Nanorods with Highly Efficient 2 μm Emission

Fátima Esteban-Betegón, Carlos Zaldo, and Concepción Cascales*

Instituto de Ciencia de Materiales de Madrid, Consejo Superior de Investigaciones Científicas, c/Sor Juana Inés de la Cruz, 3, E-28049 Madrid, Spain

Supporting Information

ABSTRACT: Cubic $Ia\bar{3}$ Tm—Lu_2O_3 porous nanorods of ~45 μm length and 90 nm diameter have been prepared with precise compositions through a soft hydrothermal route (i.e., autogenic pressure, neutral pH, and 185 °C for 24 h) by using chloride reagents. For these nanorods, room temperature excitation and photoluminescence spectra of Tm^{3+} multiplets related to the eye-safe $^3F_4 \rightarrow {}^3H_6$ laser transition at ~1.85—2.05 μm are similar to those of bulk crystals. Room-temperature luminescence decays of $^3H_4$ and $^3F_4$ exhibit nonexponential dynamics analytically reproduced by the sum of two exponential regimes, which are ascribed to the different rates of nonradiative relaxations in defects at the surface and in the body of the nanocrystals, respectively. Measured fluorescence lifetimes $\tau \sim 200$—260 μs and $\tau \sim 2.3$—2.9 ms for $^3H_4$ and $^3F_4$, respectively, in 0.2% mol Tm—Lu_2O_3 nanorods, are considerably larger than in previous nanocrystalline Tm-doped sesquioxides, and they are close to values of bulk sesquioxide crystals with equivalent Tm^{3+} content.

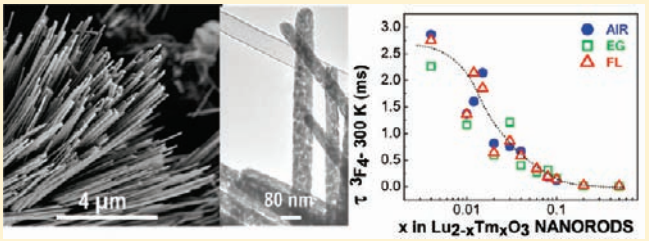

INTRODUCTION

Nanocrystalline materials based on optically active trivalent lanthanides (hereafter, Ln) are systems in which the properties derived from the specific features of the 4f electronic transitions can be highly modified via shape and dimensionality effects. Given the localized nature of 4f orbitals, changes in the local environment around Ln^{3+} centers induced by the size reduction rather than modification of the energy levels of $4f^N$ states would influence the dynamics of f—f luminescence transitions, and thus emission lifetimes, luminescence efficiency, upconversion emission characteristics, and concentration quenching are substantially affected.[1−4] In this way, nanostructures of optically active Ln^{3+} compounds would offer the possibility of acting as highly functionalized materials in nanoscale electronics, photonics, and ultrasensitive bioanalysis.[3−5] Special interest has been devoted to 1D crystalline nanostructures,[6−9] which additionally can play an important role as functional building units for the fabrication of nanodevices based in 2D or 3D ordered structures, for a wide range of photonic-related applications.

The evaluation of the optical response of Ln^{3+} embedded in nanocrystalline hosts, whose bulk counterparts are already well characterized, seems to be a rational approach to enabling the development of such novel devices. Specifically, single crystals of cubic $Ia\bar{3}$ transparent rare earth (RE) sesquioxides RE_2O_3 (RE = Sc, Y, Gd, and Lu) that combine excellent thermomechanical properties, relatively low phonon energies, and high doping admittance for Ln cations[10,11] are highly attractive hosts to use for developing Ln-based solid state lasers for high power applications. Furthermore, Ln^{3+} cations in these hosts show large optical absorption and emission cross sections and large crystal field splitting.[10] Tm^{3+} laser emission in RE_2O_3 single crystals has been demonstrated,[12−15] but the required high melting temperatures, ~2500 °C, constitute an important limitation for the production of single crystals, and thus for the development of such laser applications. As an alternative, low temperature methodologies to prepare nanocrystals of this phase, mainly intended for fabricating transparent laser ceramics,[12] are helping to solve these difficulties. Other possible applications for microcrystals and nanocrystals of Tm-doped RE_2O_3 are related to their incorporation in hybrid composites by merging, infiltration, or coating with other transparent materials.[5]

The Tm^{3+} laser channel that attracts more interest is $^3F_4 \rightarrow {}^3H_6$, operating at ~1.85—2.05 μm, due to the wide range of applications related to its eye-safe nature and favorable absorption in water.[15] Its efficient optical absorption at ~800 nm through the $^3H_6 \rightarrow {}^3H_4$ electronic transition makes pumping possible with commercially available, powerful AlGaAs diode lasers, which grants a great advantage over traditionally used 2.1 μm Ho^{3+}-doped laser crystals. Further, Tm^{3+} electronic transitions are broader than those of Ho^{3+}, which favors tunability of the continuous wave (cw) emission as well as ultrashort (fs) pulsed laser operation.[16] The similar mass, size, and electronic configuration of Lu_2O_3 makes this host the right choice for favorable incorporation of the highest concentrations of Tm^{3+}, with an absorption and emission cross section larger than in the more usual Y_2O_3 matrix.[10]

Received: October 4, 2010
Published: March 02, 2011

Currently, by using a large variety of methods and experimental conditions, nanosized pure or RE-doped (mainly Eu) Lu_2O_3 crystals with diverse morphologies have been prepared, which in the most cases consist of more or less agglomerated nanoparticles.[17−22] More scarce are the preparations yielding well-defined 1D,[23−25] 2D,[24] or 3D[26,27] architectures. Among all of these methods, mild hydrothermal routes allow for the successful preparation of well-defined compositions, with adequate control over the phase purity and morphology of the desired material, aspects that have been demonstrated to be crucial for high luminescence performance.[28] Taking into account the special interest in applications of optically active 1D crystalline nanostructures, for waveguiding purposes or for their incorporation as functional building units in 2D and 3D patterned photonic structures, this work presents results of the preparation of precise compositions of pure cubic $Ia\bar{3}$ Tm−Lu_2O_3 nanorods by using a highly efficient and low cost process, a template-free, soft (autogenic pressure, low temperature, neutral pH) hydrothermal route. However, along with benefits provided by hydrothermal processing, which include a benign environment and scalability, often the emission properties of Ln nanocrystals are strongly changed[29] when compared to the high-temperature prepared bulk single crystal counterparts. Consequently, the second part of our study is devoted to the evaluation of Tm^{3+} optical emission in the eye-safe 2 μm wavelength region for prepared Tm^{3+}-doped Lu_2O_3 nanorods. This analysis is carried out by room temperature measurements of the photoluminescence spectra as well as fluorescence lifetimes of $^3H_4$ and $^3F_4$ Tm^{3+} multiplets for nanorods with several Tm^{3+} concentrations, and then the results are compared with corresponding data from counterpart bulk crystals.[10,30,31]

EXPERIMENTAL SECTION

Sample Preparation. A series of samples of composition $Lu_{2-x}Tm_xO_3$ ($0.004 \leq x \leq 0.5$), i.e., with a Tm^{3+} concentration [Tm] ranging from 0.2 to 25 mol %, has been hydrothermally prepared using the corresponding stoichiometric molar amounts of sesquioxides Lu_2O_3 and Tm_2O_3 (WuXi YiFeng Rare Earth Co Ltd., 99.99%) that were first dissolved under heating in a dilute HCl solution (10 mL of distilled water and 5 mL of 38 wt % HCl). After complete evaporation, 20 mL of distilled water was added to form a clear solution, and then the pH was adjusted to 7 by the addition of dilute NH_4OH. The obtained white suspensions were subsequently heated at 185 °C for 24 h in Teflon-lined autoclaves of 75 mL capacity. The white precipitate resulting from the hydrothermal reaction, the hydrothermal precursor (**P**), was separated by centrifugation and washed with deionized water several times, dried, and then annealed to 800 °C over 30 min to obtain the Tm-doped Lu_2O_3 sesquioxide (**S**).

Characterization of Hydrothermal and Annealed Samples. The phase of each **P** and the purity of corresponding **S** were tested using 300 K powder X-ray diffraction (XRD) performed in a Bruker AXS D-8 Advance diffractometer, using Cu Kα radiation.

Field emission scanning electron microscopy (FE-SEM) images were taken with a FEI NOVA SEM230 microscope with an accelerating voltage of 5−7 kV. Transmission electron microscopy (TEM) images were recorded with a JEOL 2000FXII microscope with an accelerating voltage of 200 kV.

KBr (Strem Chemicals, 99.999% in K, kept during 20 h at 400 °C) was used to prepare pellets of the nanocrystalline sesquioxides, and corresponding Fourier transform infrared absorption (FT-IR) data were collected on a Nicolet 20SXC spectrophotometer in the range 4000−250 cm^{-1}.

Micromeritics Flowsorb 2300 and Micromeritics ASAP 2010 equipment was used for N_2 adsorption and N_2 adsorption/desorption isotherm measurements, respectively, performed at 77 K. Specific surface and size pore distribution were determined from Brunauer−Emmet−Teller (BET) and Barret−Joyner−Halenda (BJH) calculations, respectively.

Tm^{3+} fluorescence was excited at room temperature with a Quanta-Ray MOPO-HF optical parametric oscillator. This tunable laser system provides optical pulses shorter than 5 ns from 700 to 1750 nm. The pulse energy at λ = 802 nm was ∼32 mJ. The fluorescence was dispersed by a single grating SPEX spectrometer (f = 34 cm) and measured with a Hamamatsu InP/InGaAs cooled (−60 °C) photomultiplier, model H9170-75, sensitive in the 950−1700 nm range with a rise time of 0.9 ns, or by an InAs Hamamatsu photovoltaic detector cooled to liquid nitrogen temperature and sensitive in the 1500−3100 nm range with a rise time of 0.1 μs. The electrical signals were recorded either with a lock-in amplifier for emission and excitation spectra or with a 500 MHz Tektronix oscilloscope, model TDS-520, for lifetime measurements. A long-wavelength pass filter with a cutting edge at 1000 nm was used to remove background excitation light. The radiative lifetime of Tm^{3+} in nanocrystals with sizes smaller than ∼15 nm can be influenced by the refractive index of the surrounding media. To estimate such influence and assess the validity of the results, we measured the lifetime τ of nanocrystalline $Lu_{2-x}Tm_xO_3$ dispersed in infrared transparent media with increasing refractive index (n): liquid ethylene glycol (EG), n = 1.52; solid KBr, n = 1.53−1.54; or fluorolube (liquid Polychlorotrifluoroethylene, FL), n = 1.94.

RESULTS AND DISCUSSION

Crystal Phase Characterization of Prepared Materials. The Lu_2O_3 lattice crystallizes with the cubic c-type structure, also known as bixbyte, which belongs to the space group $Ia\bar{3}$.[32] This lattice has two distinct crystallographic sites for Lu^{3+}, with C_2 and C_{3i} point symmetries, see the Figure 1a, in a 3:1 ratio in the unit cell, which are available for Tm^{3+} substitution. In general, RE^{3+} cations have been found to be randomly distributed over both sites in this structure.[33] According to selection rules, the electric dipole transitions are forbidden from Tm^{3+} occupying C_{3i} sites due to its associated inversion center. In the section concerning Tm^{3+} emission properties, it will be assumed that the optical spectra show electric dipole transitions corresponding to Tm^{3+} ions located in C_2 sites and magnetic dipole transition from Tm^{3+} in both kinds of sites.

As an example, XRD patterns of **P** and the final **S** $Lu_{1.99}Tm_{0.01}O_3$ obtained after annealing the latter are shown in Figure 2a and b, respectively. **P** contains a mixture of crystal phases, but given that studies on solution-derived Lu compounds are scarce compared with those of other Ln's, their precise identification is somewhat complex. It is possible, however, to distinguish the presence of two hexagonal $P6_3/m$ phases, the first one isostructural to $RE(OH)_3$, even if the existence of this phase has been previously limited to La−Tm compounds,[34] and the other isostructural to $Er(ClO_4)_3$.[35] The final product is always the pure cubic $Ia\bar{3}$ phase.[36] A mean particle size of a ∼25 nm is calculated for **S** from the full-width at half-maximum (fwhm) of broadened Bragg peaks by using the Debye−Scherrer formula assuming spherical particles.

For the series of prepared $Lu_{2-x}Tm_xO_3$ compounds with $0.004 \leq x \leq 0.10$ compounds, the evolution of the unit cell parameter of the cubic phase, determined from Rietveld refinements[37] of their XRD profiles, shows an increase with the Tm^{3+} incorporation in the Lu_2O_3 host that ranges from

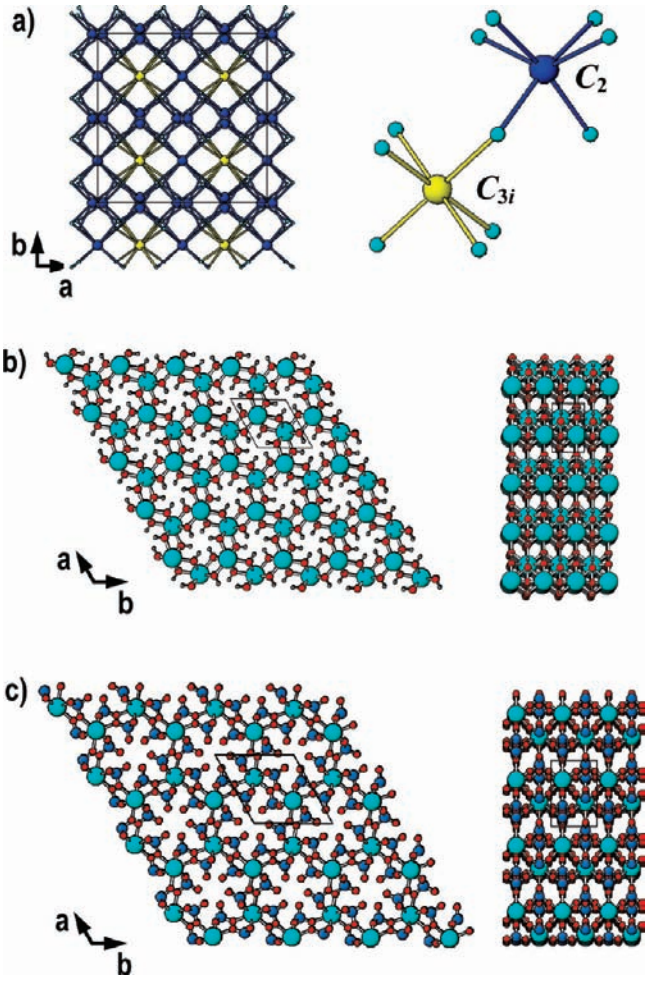

Figure 1. (a) View of the *ab* plane of cubic Lu_2O_3, with the two LuO_6 coordination polyhedra with point symmetries C_{3i} (yellow) and C_2 (blue). Views of hexagonal $P6_3/m$ quasi-layered structures of (b) $RE(OH)_3$ and (c) $Er(ClO_4)_3$, in the *ab* plane (left), and along the *c* axis (right). Cyan, red, gray, and blue balls represent Er, O, H, and Cl atoms, respectively.

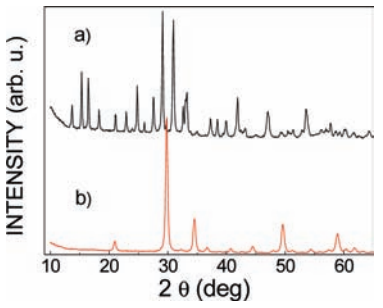

Figure 2. X-ray diffraction patterns of products of hydrothermal syntheses. (a) Precursor **P** and (b) $Lu_{1.99}Tm_{0.01}O_3$ **S**.

a = 10.392(2) Å (*x* = 0.004) to 10.397(2) Å (*x* = 0.1). This evolution agrees with crystallographic data for both extreme members of the series, i.e., stoichiometric Lu_2O_3 (*a* = 10.391(5) Å) and Tm_2O_3 (*a* = 10.488(6) Å).[38]

The room temperature FT-IR spectrum for prepared $Lu_{1.99}Tm_{0.01}O_3$ is displayed in Figure 3. Bands observed from ~305 cm^{-1} to 605 cm^{-1} are basically the same as those described and

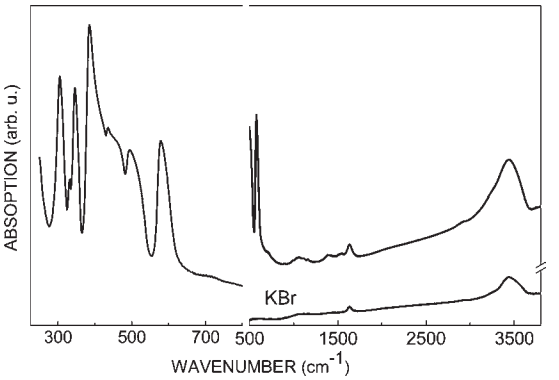

Figure 3. Room temperature FT-IR spectra of nanocrystalline $Lu_{1.99}Tm_{0.01}O_3$. The spectrum of KBr used for preparing pellets (blue line) is shown at the bottom (right part) for reference.

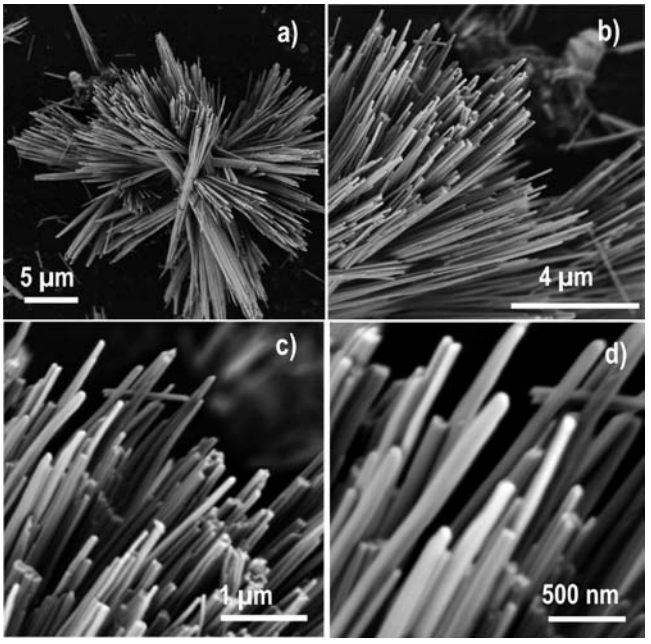

Figure 4. FE-SEM images of the hydrothermal precursor **P** (pH = 7 controlled with NH_4OH) of $Tm-Lu_2O_3$ sesquioxide: sheaves of nanorods of ~45 μm in length and ~90 nm Ø.

assigned to modes of skeletal vibrations of Lu_2O_3.[39] Bands centered at 1630 cm^{-1} and at ~3440 cm^{-1} correspond to HOH bending modes and to OH^- stretching vibrations of lattice water, respectively,[40] but since they are also observed in a blank KBr pellet, we can suppose that they are related to some extent with the used KBr. Extremely weak bands observed at ~1400 cm^{-1} and ~1530 cm^{-1} can be assigned to the symmetric and antisymmetric stretching vibrations of surface-adsorbed carboxylate ions.[40,41]

Morphology of Hydrothermal Precursor and Tm^{3+}-Doped Lu_2O_3 Materials. Figure 4 shows a panel of representative FE-SEM images of **P** obtained by adjusting the pH (= 7) with NH_4OH. The morphology can be described as consisting of rods up to ~45 μm in length and 90 nm in diameter, which are gathered forming sheaves tied in the middle. These nanorods are uniform, with smooth surfaces.

Hexagonal $P6_3/m$ phases isostructural to $Er(OH)_3$ and $Er(ClO_4)_3$ identified in **P** possess quasi-layered structures in the *ab* plane, with 6-rings of REO_6 octahedra sharing edges along the *c*

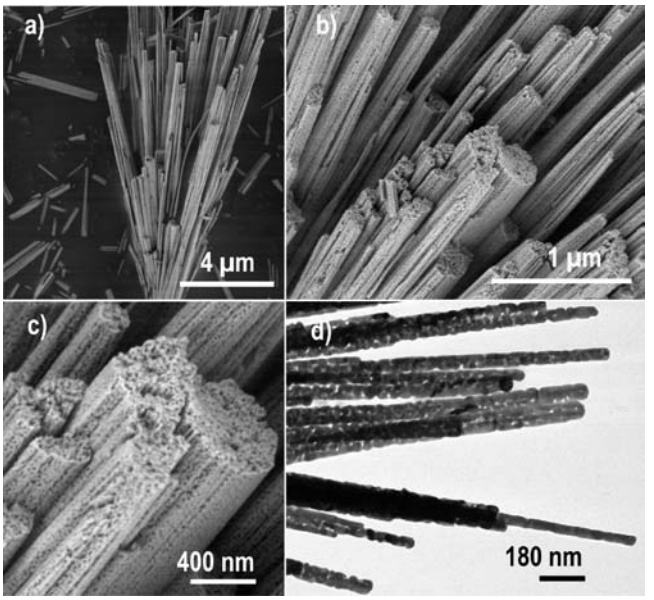

Figure 5. Micrographs of Tm−Lu_2O_3 obtained by annealing the hydrothermal precursor **P** to 800 °C: (a, b, c) FE-SEM images of thicker assemblies of porous nanorods and (d) TEM image of porous nanorods.

axis, see Figure 1b,c, and they can grow with 2D shape under specific hydrothermal conditions.[42] The 1D morphology in **P** is plausibly achieved by a rolling up process acting on the hydrothermally formed layered structures, and then this initial nanostructure operates as the driving force for the growth of nanorods,[43] which under the specific reaction conditions agglomerate to form the current micrometer-sized sheaves tied at the center.[44]

The sesquioxide **S** prepared by thermal annealing of the above precursor inherits the microstructure of **P**, see FE-SEM images in Figure 5. Nanorods forming the sheaves coalesce to some extent, forming thicker assemblies as shown in Figure 5a−c. The main morphological difference is, however, the important porosity induced by the removal of anionic groups from the **P** frameworks, as revealed by SEM image in Figure 5c and TEM images in Figures 5d and 6a,b. The rods are constituted of attached pseudo-hexagon-shaped nanoparticles with a size of ∼20 nm per side, consistent with results from the XRD analysis. Furthermore, quasi-spherical nanocrystals of ∼10 nm and free pseudo-hexagon-shaped nanoparticles with sizes from 20 to 50 nm also appear in TEM images of Figure 6c−e. The simulation of the shape[45] of polyhedral Tm−Lu_2O_3 nanoparticles indicates that their aspect is mainly determined by the relationship between the growth rates along the ⟨100⟩ and ⟨110⟩ directions of the cubic Lu_2O_3 structure, see insets in Figure 6d,e. This growth is clearly different from that described for colloidal cubooctahedra nanoparticles of cubic $Fm\bar{3}m$ CeO_2, which instead develop {100} and {111} facets in the absence of selective passivating surface adsorption.[46]

Spectroscopic Properties. A scheme of the energy levels of Tm^{3+} in Lu_2O_3 with the relevant energy transfer processes related to the "eye safe" $^3F_4 \rightarrow {}^3H_6$ laser transition operating at ∼1.85−2.05 μm can be seen in Figure S1a of the Supporting Information.

In a first step, we monitored the room temperature optical absorption of crystalline Tm−Lu_2O_3 nanorods through the excitation spectrum of the infrared fluorescence, see Figure S1b (Supporting Information) for some selected compositions. Then,

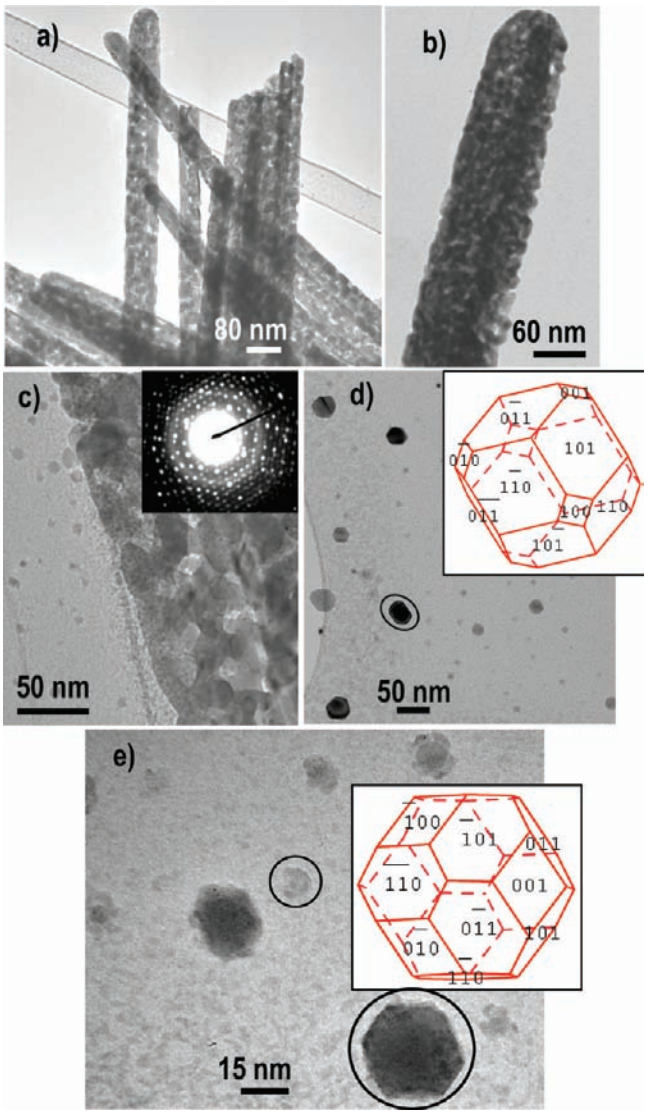

Figure 6. TEM micrographs with details of Tm−Lu_2O_3 nanorods: (a, b, c) Images showing the porous nanorods and the pseudo-hexagon-shaped nanocrystals that form these rods. (d) Free individual hexagon-shaped and quasi-spherical nanocrystals in Tm−Lu_2O_3. (e) The smallest observed Tm−Lu_2O_3 nanocrystals. (Top right inset in c) SAED image in a rod. (Top right insets in d and e) SHAPE[45] simulations of the crystal growth habit for nanocrystals of Tm−Lu_2O_3.

exciting close to the maximum of $^3H_6 \rightarrow {}^3H_4$, λ_{exc}∼800 nm, the fluorescence bands associated with electronic transitions $^3H_4 \rightarrow {}^3F_4$ ($\lambda \approx$ 1400−1600 nm) and $^3F_4 \rightarrow {}^3H_6$ ($\lambda \approx$ 1600−2200 nm) were collected, Figures S1c and S2 (Supporting Information), respectively. These spectra were similar for all tested Tm^{3+} compositions, see Figures S2 (Supporting Information) corresponding to 300 K $^3F_4 \rightarrow {}^3H_6$ photoluminescence (PL), λ_{EXC} = 802 nm spectra of several prepared $Lu_{2-x}Tm_xO_3$ nanorods. These optical transitions display splittings very similar to those reported for Tm^{3+}-doped single crystals,[10,13,14] indicating that in prepared sesquioxides Tm^{3+} is actually incorporated at the same crystal site(s) as in single crystals. Furthermore, the position of Tm^{3+} energy levels does not seem affected by the morphology. However, possible changes in the local structure around Tm^{3+} cannot be discarded, and some broadening is observed in PL spectra.[13] Moreover, the overall intensity

of PL emissions in Tm−Lu_2O_3 nanorods appears to be reduced in comparison with usual results yielded by bulk crystals.[10] Although the lower apparent density of the nanocrystalline material with regard to bulk samples could explain the latter behavior, the reduction of the size and the presence of a higher density of defects in the surface of nanocrystals, as well as possible interactions with phonon modes in the close environment of Tm^{3+} centers, would induce modifications in the dynamics of f−f luminescence transitions. Lifetime measurements are able to monitor such modifications.

The lifetime of the $^3F_4$ multiplet can only be experimentally tested through relaxation to the ground $^3H_6$ multiplet, which is electronically populated at room temperature. Thus, the self-absorption of the photoluminescence and its re-emission may lead to an artificial retardation of the measured light decay, which is more noticeable as the Tm^{3+} concentration increases. On the other hand, a strong reduction of the lifetime is expected with the increase of the Tm^{3+} concentration.[10,30] Consequently, the experimental values obtained in Tm^{3+} concentrated media usually do not represent the true lifetime of this multiplet. Although several methods can be used to minimize this effect, we will first measure the $^3H_4 \rightarrow {}^3F_4$ transition lifetime, which can be considered free of fluorescence reabsorption, by using low concentrated samples.

$^3H_4$ Lifetime in Tm−Lu_2O_3 Nanorods. The 300 K $^3H_4 \rightarrow {}^3F_4$ photoluminesce decays excited at 802 nm were independent of the emission wavelength (λ_{EMI} = 1370−1600 nm) monitored. None of these decays is exponential, even for the most diluted prepared sample, x = 0.004, see Figure 7. The time dependence of the photoluminescence intensity of Tm^{3+}−Lu_2O_3 nanorods is different from that known in RE_2O_3 (RE = Y, Lu) single crystals,[10,30] in which, for low enough Tm^{3+} concentrations (typically <0.5 × 10^{19} cm^{-3}), $^3H_4$ decays are exponential, followed by a complex behavior above this concentration due to Tm−Tm interactions, including resonant transfer between $^3H_4$ multiplets and $^3H_4$−$^3F_4$ cross-relaxation, recovering again the exponential relaxation when the increase of the Tm^{3+} concentration (~3 × 10^{20} cm^{-3}) allows

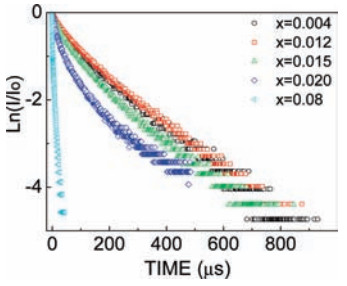

Figure 7. 300 K Photoluminescence intensity decay of the $^3H_4$ multiplet of Tm^{3+} for different x contents in $Lu_{2-x}Tm_xO_3$ nanorods immersed in fluorolube (n = 1.94). λ_{EXC}= 802 nm, λ_{EMI}= 1446 nm.

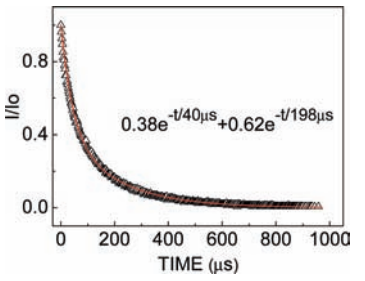

Figure 8. The 300 K photoluminescence intensity decay of the $^3H_4$ multiplet of Tm^{3+} in $Lu_{1.985}Tm_{0.015}O_3$ (0.75% Tm) nanorods dispersed in fluorolube. λ_{EXC} = 802 nm, λ_{EMI} = 1446 nm. The points are the experimental results, and the continuous line is the fit with two exponential decays of the I/I_o vs time plot.

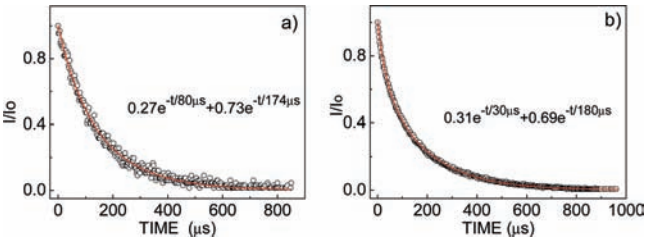

Figure 9. The 300 K photoluminescence intensity decay of the $^3H_4$ multiplet of Tm^{3+} in $Lu_{1.988}Tm_{0.012}O_3$ (0.6% Tm) nanorods dispersed in (a) ethylene glycol and (b) fluorolube. λ_{EXC} = 802 nm, λ_{EMI} = 1446 nm. The points are the experimental results, and continuous lines are the fits with two exponential decays of the I/I_o vs time plot.

Table 1. The 300 K Experimental Lifetimes (τ, μs) and Intensities (I) of the $^3H_4$ De-Excitation of $Lu_{2-x}Tm_xO_3$ Nanorods from Fits of $I(t) = I_1\, e^{-t/\tau 1} + I_2\, e^{-t/\tau 2}$ ($I_1 + I_2 = 1$; λ_{EXC} = 802 nm, λ_{EMI} = 1446 nm)

	EG (n = 1.52)				KBr (n = 1.54)				FL (n = 1.94)			
x	I_1	τ_1	I_2	τ_2	I_1	τ_1	I_2	τ_2	I_1	τ_1	I_2	τ_2
0.004	0.46	11	0.54	230	0.54	50	0.46	245	0.36	30	0.64	196
0.010	0.55	30	0.44	160								
0.012	0.27	80	0.73	174	0.57	70	0.43	257	0.31	30	0.69	180
0.015	0.26	20	0.74	143	0.37	50	0.63	202	0.38	40	0.62	198
0.02	0.68	40	0.32	140	0.62	20	0.38	117	0.69	20	0.31	172
0.03	0.50	20	0.50	97	0.70	10	0.30	82	0.68	20	0.32	92
0.04	0.71	7.3	0.29	40	0.69	7.7	0.31	38	0.66	9	0.34	38
0.06	0.64	3.7	0.36	16	0.67	3	0.33	17	0.72	3.5	0.28	20
0.08	0.57	1.5	0.43	8	0.69	1.3	0.31	8.8	0.70	2.3	0.30	11
0.10	0.62	0.8	0.38	5	0.72	1.7	0.28	7.9	0.69	1.5	0.31	7.5
0.20	0.72	0.1	0.28	0.8	0.81	0.2	0.19	1.25	0.77	0.16	0.23	1.1
0.50	0.76	0.01	0.24	0.07	0.89	0.02	0.11	0.09	0.94	0.05	0.06	0.73

dx.doi.org/10.1021/ic102022t |*Inorg. Chem.* 2011, 50, 2836–2843

fast diffusion between excited $^3H_4$ multiplets. Thus, $^3H_4$ decays of Tm^{3+}—Lu_2O_3 nanorods have been fitted with a double exponential model, $I(t) = I_1\, e^{-t/\tau 1} + I_2\, e^{-t/\tau 2}$, with $I_1 + I_2 = 1$. The fast component at short times would correspond to the emission of Tm^{3+} ions at the surface of nanocrystals, and the long one (evaluated first from the tail of the $Ln(I/I_0)$ vs time decay plot) to Tm^{3+} ions within the body of nanocrystals, which in principle should approach the lifetime value obtained in Tm^{3+}—Lu_2O_3 single crystals. Such a procedure has systematically produced good fits of our experimental photoluminescence decays; see as an example the fit shown in Figure 8 for $Lu_{1.985}Tm_{0.015}O_3$ (0.75% Tm) nanorods.

Measurements carried out dispersing Tm^{3+}—Lu_2O_3 nanocrystals in ethylene glycol (EG), KBr, and fluorolube (FL) do not allow for the detection of any systematic dependence of the long-lived $^3H_4$ lifetime on these surrounding media,[47] see Figure 9a,b for 0.6% Tm—Lu_2O_3 nanorods measured in EG and FL. This is most likely due to the aggregation of the primary nanoparticles of ~20 nm into nanorods.

Table 1 presents a comparison of the results obtained for $Lu_{2-x}Tm_xO_3$ nanorods, and Figure 10 shows an overview of the long-lived lifetime dependence with the Tm^{3+} concentration. Along with the usual progressive fastening of $^3H_4$ decay transients with the increase in the Tm^{3+} concentration, an important development of their short time component occurs, with very pronounced short time components appearing already for x = 0.02, i.e., for 1% mol Tm. Obtained $^3H_4$ long-lived lifetimes progressively increase for lower Tm^{3+} concentrations, varying from 7 μs (x = 0.10, 5% Tm^{3+}) up to τ ~260 μs. This latter value represents a reduction with regard to measured $^3H_4$ lifetime in

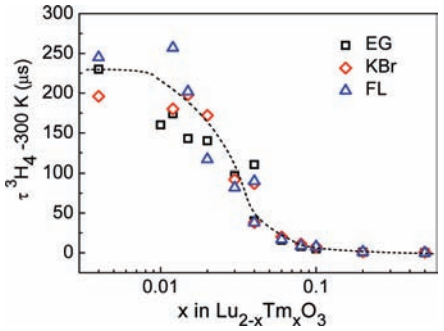

Figure 10. Dependence on the Tm^{3+} content of the 300 K long-lived $^3H_4$ lifetime in $Lu_{2-x}Tm_xO_3$ nanorods. λ_{EXC} = 802 nm, λ_{EMI} = 1446 nm. Samples measured in ethylene glycol (EG) (squares), KBr (diamonds), and fluorolube (FL) (triangles).

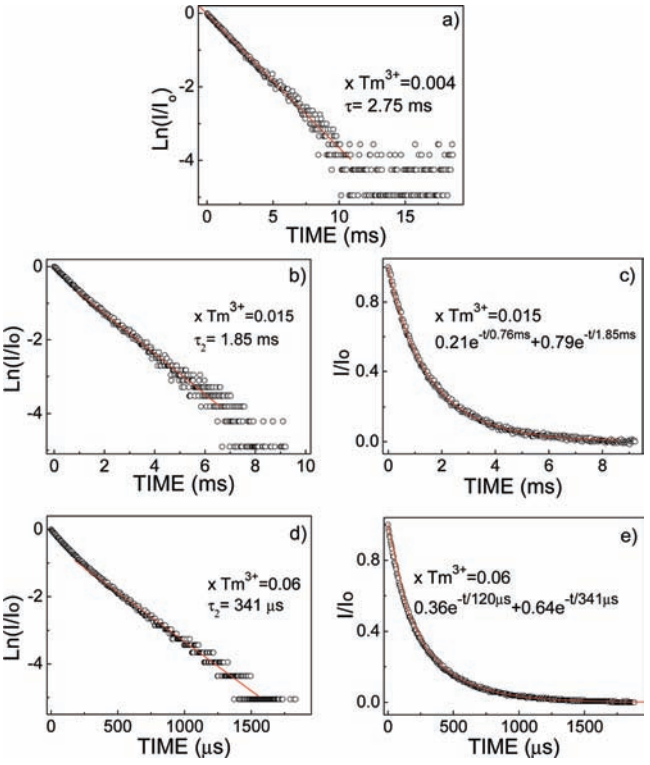

Figure 11. Evolution with the Tm^{3+} content of the 300 K photoluminescence intensity decay of the $^3F_4$ multiplet of Tm^{3+} in $Lu_{2-x}Tm_xO_3$ nanorods measured in fluorolube: (a) x = 0.004, 0.2% Tm^{3+}; (b and c) x = 0.015, 0.75% Tm^{3+}; (d and e) x = 0.06, 3% Tm^{3+}. λ_{EXC} = 802 nm, λ_{EMI} = 1636 nm. The points are the experimental results, and the continuous lines are (a, b, d) the linear fit of the tail of the $Ln(I/I_o)$ vs time plot and (c, e) the fit with two exponential decays of the I/I_o vs time plot.

Table 2. The 300 K Experimental Lifetimes (τ, ms) and Intensities (I) of the $^3F_4$ De-Excitation of $Lu_{2-x}Tm_xO_3$ Nanorods from Fits of $I(t) = I_1\, e^{-t/\tau 1} + I_2\, e^{-t/\tau 2}$ ($I_1 + I_2 = 1$; λ_{EXC} = 802 nm, λ_{EMI} = 1960 nm in the Air and λ_{EMI} = 1636 nm in Ethylene Glycol (EG) or in Fluorolube (FL))

	air (n = 1)				EG (n = 1.52)				FL (n = 1.94)			
x	I_1	τ_1	I_2	τ_2	I_1	τ_1	I_2	τ_2	I_1	τ_1	I_2	τ_2
0.004	0.34	0.76	0.66	2.86	0.11	0.23	0.94	2.26			1	2.75
0.010	0.37	0.40	0.63	1.37	0.35	0.12	0.65	1.16			1	1.36
0.012			1	1.60		weak signal					1	2.14
0.015	0.58	0.62	0.42	2.14		weak signal			0.21	0.76	0.79	1.85
0.02	0.19	0.23	0.81	0.81	0.35	0.07	0.65	0.59			1	0.64
0.03	0.19	0.25	0.81	0.76	0.31	0.27	0.69	1.21	0.26	0.24	0.74	0.86
0.04	0.52	0.22	0.48	0.66	0.42	0.08	0.58	0.40	0.49	0.19	0.51	0.58
0.06	0.31	0.05	0.69	0.32			1	0.27	0.36	0.12	0.64	0.34
0.08	0.33	0.03	0.67	0.18	0.51	0.13	0.49	0.32			1	0.19
0.10	0.37	0.04	0.63	0.12	0.41	0.03	0.59	0.15	0.31	0.50	0.69	0.14
0.20			1	0.02			1	0.01	0.25	0.01	0.75	0.02
0.50			1	0.01			1	0.001	0.98	0.001	0.02	0.01

dx.doi.org/10.1021/ic102022t |Inorg. Chem. 2011, 50, 2836–2843

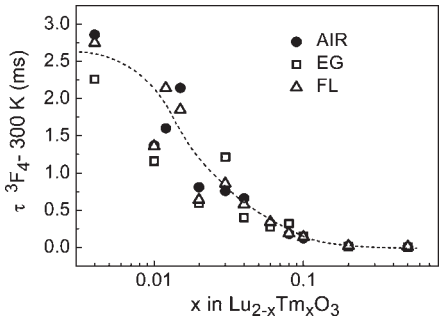

Figure 12. Dependence on the Tm^{3+} content of the 300 K long-lived $^3F_4$ lifetime in $Lu_{2-x}Tm_xO_3$ nanorods. λ_{EXC}= 802 nm, λ_{EMI} = 1636 nm (open symbols) and λ_{EMI} = 1960 nm (full symbols). Samples measured in air (circles), ethylene glycol (EG; squares), and fluorolube (FL; triangles).

single crystals, 310 μs for isostructural 0.25% Tm−Y_2O_3[30] and 350 μs for 0.15% Tm−Lu_2O_3.[10] However, the τ = 172 μs value obtained (FL) for our 1% Tm^{3+}−Lu_2O_3 nanorods nearly converges with lifetime values in single crystals with the same Tm^{3+} doping level, τ = 190 μs in Y_2O_3[31] and τ = 181 μs in Lu_2O_3,[10] being considerably larger than the reported τ = 94 μs for previous nanocrystalline 1% Tm−Y_2O_3 prepared from a propellant synthesis.[48]

$^3F_4$ Lifetime in $Lu_{2-x}Tm_xO_3$ Nanorods. Since the $^3F_4$ photoluminescence is excited through the $^3H_4$ multiplet, the fluorescence intensity initially grows corresponding to its electronic charge; thus the signal for times shorter than twice the $^3H_4$ lifetime was neglected. The rest of the decay was analyzed in the same way as for $^3H_4$ decays. Although lower concentrated samples ($x \leq 0.010$, 0.5% Tm^{3+}) display mostly a single exponential decay regime, $^3F_4$ photoluminescence decays of $Lu_{2-x}Tm_xO_3$ nanorods are, in general, non-single-exponential, see Figure 11 a−e, showing the indicated evolution in samples with x = 0.004, 0.015, and 0.06 (0.2%, 0.75%, and 3% Tm^{3+}, respectively) immersed in FL.

Table 2 shows the results obtained for $Lu_{2-x}Tm_xO_3$ nanorods in different media, and Figure 12 shows the evolution of long-lived $^3F_4$ lifetimes with the Tm^{3+} content. The maximum value of the long-lived lifetime measured for the lowest (x = 0.004, 0.2%) Tm^{3+} concentration was $\tau \sim 2.9$ ms, which is close to the $\tau \sim 3.38$ ms experimental lifetime reported at 300 K for a 0.15% mol Tm−Lu_2O_3 single crystal.[10] Both values are considerably lower than the calculated $^3F_4$ radiative value τ = 5.22 ms.[10] Although Tm−Tm interactions can be ignored for such low Tm^{3+} concentrations, the likely origin of these reductions is a nonradiative probability of intraionic up-conversion giving rise to strong temperature dependence, which decreases the lifetime measured at room temperature with regard to its value at 10 K.[49]

The measured long-lived $^3F_4$ lifetime progressively decreases with an increase in the Tm^{3+} concentration. This reflects that Tm−Tm interactions are strongly contributing to non-radiative processes, including energy migration by fast diffusion, and indicates an apparently small influence of the fluorescence reabsorption in our measurements.

CONCLUSIONS

The control of the reaction conditions in a simple and soft hydrothermal process allows for obtaining well-defined morphologies for Tm^{3+}-doped Lu_2O_3 materials for specific photonic applications. In particular, crystalline nanorods currently prepared from chloride reagents at 185 °C in a pH = 7 dispersion medium can be the choice when waveguiding purposes are envisaged, or for their incorporation in 2D and 3D patterned structures. Related to the ∼2 μm laser emission, both $^3H_4$ and $^3F_4$ luminescence decays of Tm^{3+} in $Lu_{2-x}Tm_x$ O_3 nanorods show nonexponential dynamics, which can be analytically reproduced by the sum of two exponential regimes. These regimes are ascribed to the different rates of nonradiative relaxations in defects at the surface and in the body of the nanocrystals, respectively. $^3H_4$ and $^3F_4$ long-lived lifetimes measured in the lower concentrated 0.2% mol Tm^{3+} material τ = 200−300 μs and τ = 2.3−2.9 ms, respectively, are shorter than expected radiative values, 690 μs and 5.22 ms, respectively, but comparable to measured lifetimes in Lu_2O_3 single crystals with a similar Tm^{3+} doping level, τ = 350 μs and τ = 3.38 ms, respectively. Differences with radiative values are attributed to the presence of structural point defects and to small amounts of adsorbed H_2O or carboxilate ions on the nanoparticle surface, where the excitation can be relaxed by nonradiative processes. On the other hand, it is interesting to note that the largest source of nonradiative processes in Tm^{3+} concentrated bulk crystals is the fast diffusion. This mechanism could be prevented in nanocrystals due to the presence of particle frontiers leading to a lifetime recovery. However, such an effect is not observed in the studied $Lu_{2-x}Tm_xO_3$ nanocrystals. The most likely reason is the aggregation of the primary nucleus with sizes of 20 nm, and eventually some interdiffusion between them, which also provides the mechanical strength required to support long range dimension of the nanorods.

ASSOCIATED CONTENT

Supporting Information. Figure S1: (a) Scheme of energy levels of Tm^{3+} in Lu_2O_3, showing relevant energy transfer processes for the $^3F_4 \rightarrow {}^3H_6$ laser emission operating at ∼2 μm. (b) 300 K excitation spectrum (λ_{EMI} = 1962 nm) of the $^3H_4$ multiplet of $Lu_{2-x}Tm_xO_3$ nanorods. (c) 300 K $^3H_4 \rightarrow {}^3F_4$ photoluminescence (λ_{EXC} = 802 nm) spectra of $Lu_{1.996}Tm_{0.004}O_3$ nanorods. Figure S2: 300 K $^3F_4 \rightarrow {}^3H_6$ photoluminescence (λ_{EXC} = 802 nm) spectra of $Lu_{2-x}Tm_xO_3$ nanorods ($0.004 \leq x \leq 0.1$). This material is available free of charge via the Internet at http://pubs.acs.org.

AUTHOR INFORMATION

Corresponding Author
*E-mail ccascales@icmm.csic.es.

ACKNOWLEDGMENT

This work was supported by the Spanish Project MAT2008-06729-C02-01.

REFERENCES

(1) Liu, G.; Chen, X. . In *Handbook on the Physics and Chemistry of Rare Earths*; Gschneidner, K. A., Jr., Bünzli, J.-C. G., Pecharsky, V. K., Eds.; Elsevier B.V.: Amsterdam, 2007; vol 37, Chapter 233.

(2) Vetrone, F.; Boyer, J. C.; Capobianco, J. A.; Speghini, A.; Bettinelli, M. *J. Phys. Chem. B* **2003**, *107*, 1107.

(3) Heer, S.; Kömpe, K.; Güdel, H.-U.; Haase, M. *Adv. Mater.* **2004**, *16*, 2102.

(4) Wang, F.; Liu, X. *Chem. Soc. Rev.* **2009**, *38*, 976.
(5) Bridot, J. L.; Faure, A. C.; Laurent, S.; Rivière, C.; Billotey, C.; Hiba, B.; Janier, M.; Josserand, V.; Coll, J. L.; Elst, L. V.; Muller, R.; Roux, S.; Perriat, P.; Tillement, O. *J. Am. Chem. Soc.* **2007**, *129*, 5076.
(6) Nogales, E.; Garcia, J. A.; Mendez, B.; Piqueras, J. *Appl. Phys. Lett.* **2007**, *91*, 133108.
(7) Song, H.; Yu, H. Q.; Pan, G.; Bai, X.; Dong, B.; Zhang, X. T.; Hark, S. K. *Chem. Mater.* **2008**, *20*, 4762.
(8) Dong, G.; Chi, Y.; Xiao, X.; Liu, X.; Qian, B.; Ma, Z.; Wu, E.; Zeng, H.; Chen, D.; Qiu, J. *Opt. Express* **2009**, *17* (25), 22514.
(9) Wang, L.; Li, Y. *Nano Lett.* **2006**, *6* (8), 1645.
(10) Fornasiero, L. . Ph.D. Dissertation, University of Hamburg, Hamburg, Germany, 1999.
(11) Peters, V. . Ph.D. Dissertation, University of Hamburg, Hamburg, Germany, 2001.
(12) Kaminskii, A. A. *Laser Photon. Rev.* **2007**, *1*, 93.
(13) Diening, A.; Dicks, B. M.; Heumann, E.; Meyn, J.; Petermann, K.; Huber, G. . In *Advanced Solid State Lasers*, Pollock, C., Bosenberg, W., Eds. Optical Society of America: Washington, DC, 1997; Vol. of OSA Trends in Optics and Photonics Series, paper LS1.
(14) Fornasiero, L.; Berner, N.; Dicks, B.; Mix, E.; Peters, V.; Petermann, K.; Huber, G. . In *Advanced Solid State Lasers*; Fejer, M., Injeyan, H., Keller, U., Eds.; Optical Society of America: Washington, DC, 1999; Vol. 26 of OSA Trends in Optics and Photonics, paper WD5.
(15) Scholle, K.; Lamrini, S.; Koopmann, P.; Fuhrberg, P. In *Frontiers in Guided Wave Optics and Optoelectronics*; Pal, B., Ed.; INTECH: Croatia, 2010; p 471−499; ISBN 978−953−7619−82−4.
(16) Lagatsky, A. A.; Han, X.; Serrano, M. D.; Cascales, C.; Zaldo, C.; Calvez, S.; Dawson, M. D.; Gupta, J. A.; Brown, C. T. A.; Sibbett, W. *Opt. Lett.* **2010**, *35* (18), 3027.
(17) Polizzi, S.; Bucella, S.; Speghini, A.; Vetrone, F.; Naccache, R.; Boyer, J. C.; Capobianco, J. A. *Chem. Mater.* **2004**, *16*, 1330.
(18) Trojan-Piegza, J.; Zych, E. *J. Alloys Compd.* **2004**, *380*, 118.
(19) An, L.; Zhang, J.; Liu, M.; Wang, S. *J. Am. Ceram. Soc.* **2005**, *88* (4), 10101012.
(20) Zych, E.; Hreniak, D.; Strek, W. *J. Phys. Chem B* **2002**, *106*, 3805.
(21) Zych, E.; Wójtowicz, M.; Kepinski, L.; Malecka, M. A. *Opt. Mater.* **2008**, *31*, 241.
(22) Galcerán, M.; Pujol, M. C.; Aguiló, M.; Díaz, F. *Mat. Sci. Eng. B* **2008**, *146*, 7.
(23) Jia, G.; Zheng, Y.; Liu, K.; Song, Y.; You, H.; Zhang, H. *J. Phys. Chem. C* **2009**, *113*, 153.
(24) Wang, J.; Liu, Q.; Liu, Q. *J. Mater. Chem.* **2005**, *15*, 4141.
(25) Yada, M.; Mihara, M.; Mouri, S.; Kuroki, M.; Kijima, T. *Adv. Mater.* **2002**, *14* (4), 309.
(26) Yang, J.; Li, C.; Quan, Z.; Zhang, C.; Yang, P.; Li, Y.; Yu, C.; Lin, J. *J. Phys. Chem. C* **2008**, *112*, 12777.
(27) Yada, M.; Taniguchi, C.; Torikai, T.; Watari, T.; Furuta, S.; Katsuki, H. *Adv. Mater.* **2004**, *16* (16), 1448.
(28) Esteban-Betegón, F.; Zaldo, C.; Cascales, C. *Chem. Mater.* **2010**, *22*, 2315.
(29) Barrera, E. W.; Pujol, M. C.; Díaz, F.; Choi, S. B.; Rotermund, F.; Park, K. H.; Jeong, M. S.; Cascales, C. *Nanotechnology* **2011**, *22*, 075205.
(30) Guyot, Y.; Moncorgé, R.; Merkle, L. D.; Pinto, A.; McIntosh, B.; Verdun, H. *Opt. Mater.* **1996**, *5*, 127.
(31) Ermeneux, F. S.; Goutadier, C.; Moncorgé, R.; Cohen-Adad, M.-T.; Bettinelli, M.; Cavalli, E. *Opt. Mater.* **1997**, *8*, 83.
(32) Pauling, L.; Shappell, M. D. *Z. Kristallogr.* **1930**, *75*, 128.
(33) Kisliuk, P.; Krupke, W. F.; Gruber, J. B. *J. Chem. Phys.* **1964**, *40*, 3606.
(34) Beall, G. W.; Milligan, W. O.; Wolcott, H. A. *J. Inorg. Nucl. Chem.* **1977**, *39*, 65.
(35) Wickleder, M. S.; Schaefer, W. *Z. Anorg. Allg. Chem.* **1999**, *625*, 309.
(36) Powder Diffraction File Nr. 86-2475, PCPDFWin v. 2.2, JCPDS-ICDD, 2001.
(37) Roisnel, T.; Rodriguez-Carvajal, J. WinPLOTR. http://www-llb.cea.fr/fullweb/winplotr/winplotr.htm (accessed Feb 2011).
(38) Adachi, G.; Imanaka, N. *Chem. Rev.* **1998**, *98*, 1479.
(39) Schnaak, G.; Konigstein, J. A. *J. Opt. Soc. Am.* **1970**, *60*, 1110.
(40) Nakamoto, K. *Infrared and Raman Spectra of Inorganic and Coordination Compounds*; Wiley-Interscience: New York, 1986.
(41) Gao, P.; Zhan, C.; Liu, M. *Langmuir* **2006**, *22*, 775.
(42) Wang, X.; Li, Y. *Angew. Chem.* **2002**, *41*, 4790.
(43) Wang, X.; Li, Y. *Inorg. Chem.* **2006**, *45*, 7522.
(44) Chen, L.; Xie, H; Liu, Y.; Huang, K. *J. Am. Ceram. Soc.* **2007**, *90*, 1232.
(45) Dowty, E. *SHAPE for Windows*, v.7.2.1; Shape Software: Kingsport, TN, 2006.
(46) Zhang, J.; Ohara, S.; Umetsu, M.; Naka, T.; Hatakeyama, Y.; Adschiri, T. *Adv. Mater.* **2007**, *19*, 203.
(47) Meltzer, R. S.; Feofilov, S. P.; Tissue, B.; Yuan, H. B. *Phys. Rev. B* **1999**, *60*, R14012.
(48) Vetrone, F.; Boyer, J. C.; Capobianco, J. A.; Speghini, A.; Bettinelli, M. *Nanotechnology* **2004**, *15*, 75.
(49) Cornacchia, F.; Parisi, D.; Tonelli, M. *IEEE J. Quantum Electron.* **2008**, *44*, 1076.